


# High-Frequency Fe–H and Fe–H<sub>2</sub> Modes in a *trans*-Fe( $\eta^2$ -H<sub>2</sub>)(H) Complex: A Speed Record for Nuclear Resonance Vibrational Spectroscopy

Ming-Hsi Chiang,<sup>\*,†</sup> Vladimir Pelmeshnikov,<sup>\*,†</sup> Leland B. Gee,<sup>†</sup> Yu-Chiao Liu, Chang-Chih Hsieh, Hongxin Wang, Yoshitaka Yoda, Hiroaki Matsuura, Lei Li, and Stephen P. Cramer<sup>\*</sup>

 Cite This: *Inorg. Chem.* 2021, 60, 555–559

 Read Online

ACCESS |

 Metrics & More

 Article Recommendations

 Supporting Information

**ABSTRACT:** Nuclear resonance vibrational spectroscopy (NRVS) and density functional theory (DFT) are complementary tools for studying the vibrational and geometric structures of specific isotopically labeled molecular systems. Here we apply NRVS and DFT to characterize the *trans*-[<sup>57</sup>Fe( $\eta^2$ -H<sub>2</sub>)(H)(dppe)<sub>2</sub>][BPh<sub>4</sub>] [dppe = 1,2-bis(diphenylphosphino)ethane] complex. Heretofore, most NRVS observations have centered on the spectral region below 1000 cm<sup>-1</sup>, where the <sup>57</sup>Fe signal is strongest. In this work, we show that state-of-the-art synchrotron facilities can extend the observable region to 2000 cm<sup>-1</sup> and likely beyond, in measurements that require less than 1 day. The <sup>57</sup>Fe–H stretch was revealed at 1915 cm<sup>-1</sup>, along with the asymmetric <sup>57</sup>Fe–H<sub>2</sub> stretch at 1774 cm<sup>-1</sup>. For a small fraction of the H<sub>2</sub>-dissociated product, the <sup>57</sup>Fe–H stretch was detected at 1956 cm<sup>-1</sup>. The unique sensitivity to <sup>57</sup>Fe motion and the isolated nature of the Fe–H/H<sub>2</sub> stretching modes enabled NRVS to quantitatively analyze the sample composition.

Since the discovery of the first transition-metal dihydrogen complexes,<sup>1</sup> a rich chemistry has been developed for the production and interconversion of dihydrogen and hydride species.<sup>2</sup> This information is relevant for the development of better catalysts for hydrogen conversion,<sup>3</sup> improved hydrogen storage media,<sup>4</sup> and also an understanding of hydrogenase enzymes.<sup>5–7</sup> However, characterization of metal-bound dihydrogen and hydride complexes remains a substantial challenge.<sup>8–10</sup> Because of their low electron-scattering cross section, hydrogen atoms remain challenging to observe by X-ray crystallography, unless very high resolution data are available.<sup>11</sup> M (metal)–H and M–H<sub>2</sub> stretching modes are often quite weak in IR spectra. Although they can sometimes be observed in concentrated materials, they are too weak to be seen in dilute enzymes via IR. Raman spectroscopy can sometimes be useful, but both metal hydride and dihydrogen are susceptible to photolysis.<sup>12</sup> Neutron diffraction and inelastic neutron scattering (INS) are powerful tools for hydrogen studies, but they require relatively large quantities of material (~1 mmol of hydrogen), and the latter is also subject to interferences from protons in the solvent or elsewhere in the sample.

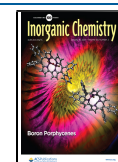
Nuclear resonance vibrational spectroscopy (NRVS)<sup>13–16</sup> has become a popular technique for elucidating the element-selective normal modes of appropriate Mössbauer isotopes.<sup>13–18</sup> In previous work, we have shown that <sup>57</sup>Fe-NRVS can be utilized to observe Fe–H bending and Fe–H–Fe(Ni) wagging modes in various model compounds<sup>19</sup> as well as intermediate species of [NiFe]<sup>20</sup> and [FeFe] hydrogenases.<sup>21–23</sup> However, to date, the only reported Fe–H stretching modes were the bands around 1230/1430 cm<sup>-1</sup> for a doubly bridging Fe( $\mu$ -H)<sub>2</sub>Fe complex<sup>24</sup> and at 1468/1532 cm<sup>-1</sup> for a singly bridging Ni( $\mu$ -H)Fe complex.<sup>20</sup> To better gauge the feasibility for observing even

higher frequency stretching modes expected for an iron-terminal hydride and dihydrogen, we have applied NRVS to examine a well-studied *trans*-[<sup>57</sup>Fe( $\eta^2$ -H<sub>2</sub>)(H)(dppe)<sub>2</sub>][BPh<sub>4</sub>] [dppe = 1,2-bis(diphenylphosphino)ethane] complex,<sup>25,26</sup> hereafter called **1**<sub>H</sub><sup>H2</sup>. As shown in Figure 1, our density functional theory (DFT) modeling of **1**<sub>H</sub><sup>H2</sup> produced an optimized structure that overlaps well with the X-ray diffraction result.<sup>26</sup> Further, we prepared the **1**<sub>H</sub><sup>D2</sup> isotopologue with diatomic deuterium, which undergoes facile intramolecular exchange with the hydride, yielding **1**<sub>D</sub><sup>HD</sup>, and then reexchanges with molecular deuterium during a 2-week incubation time under the D<sub>2</sub> atmosphere, producing **1**<sub>D</sub><sup>D2</sup>.<sup>26,27</sup> Although a series of alternative deuterium isotopologues can result from this transformation (the sample collectively called **1**-D), it, nonetheless, enables us to qualitatively identify modes pertaining to the exchangeable H and H<sub>2</sub> of the H–Fe–H<sub>2</sub> moiety in the nondeuterated NRVS sample (the sample called **1**-H). These samples were synthesized according to procedures described in the Supporting Information.

Along with the H–H stretching mode ( $\nu^{\pm}$ ), it is common to assign five normal modes for a metal complex with a side-on ( $\eta^2$ ) dihydrogen ligand, involving symmetric ( $\nu^{\uparrow\uparrow}$ ) and asymmetric ( $\nu^{\uparrow\downarrow}$ ) stretching, in-plane ( $\delta$ ) and out-of-plane ( $\delta'$ ) bending, and rotation about the M–H<sub>2</sub> axis ( $\tau^{\circ}$ ).<sup>28</sup> For **1**<sub>H</sub><sup>H2</sup>, these Fe–H<sub>2</sub>

Received: October 9, 2020

Published: December 23, 2020



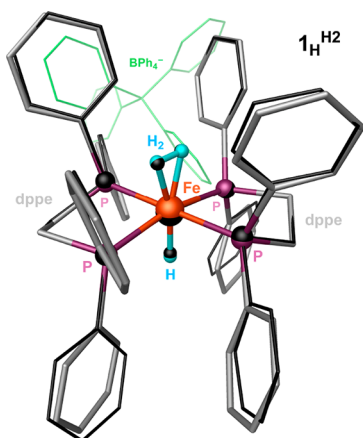


**Figure 1.** Molecular X-ray structure<sup>26</sup> of  $1_{\text{H}}^{\text{H}_2}$  (in black, with the  $\text{BPh}_4^-$  counterion shown in green) superimposed with its optimized DFT model (colored elements). The hydrogen-to-deuterium exchangeable atoms of the model structure are shown in light blue, and the rest of the hydrogen atoms are omitted for clarity.

modes will be split by coupling with Fe–H motions, as shown in Chart 1 for a minimal  $C_{2v}$ -symmetric DFT model  $1_{\text{H}}^{\text{H}_2-C_{2v}}$ . Of course, a complete analysis needs to consider interactions with the dppe ligands. The modes illustrated in Chart 1, nevertheless, provide a good starting point for the interpretation of our NRVS spectra.

Solid-state NRVS spectra for samples 1-H and 1-D in the high-frequency range are compared with each other and with the corresponding DFT  $^{57}\text{Fe}$ -PVDOS (partial vibrational density of states) simulations in Figure 2a,b. All of the modes expected for  $1_{\text{H}}^{\text{H}_2}$  in this region (Table S1), as well as the bands attributed to dissociation (loss of  $\text{H}_2$  forming  $1_{\text{H}}^*$ ) or substitution (exchange of  $\text{H}_2$  by  $\text{N}_2$  called  $1_{\text{H}}^{\text{N}_2}$ ) byproducts, are readily assigned; see Figures S2 and S6–S7 for their DFT structures and individual spectra.<sup>26,27</sup> Starting at the low-frequency end, an isotopically sensitive band at  $1052\text{ cm}^{-1}$  is assigned to the symmetric Fe– $\text{H}_2$  stretch ( $\nu^{\uparrow\uparrow}$ ); see the arrow-style representations in Figure 2, top. Animations showing DFT-calculated normal modes with significant (>10%) contributions of either  $^{57}\text{Fe}$  or iron-bound proton PVDOS are available as part of the Supporting Information.

There is a shoulder in the data at  $\sim 1080\text{ cm}^{-1}$ , identified as  $\nu^{\uparrow\uparrow}$  mixed with ligand Ph–H bending. The corresponding

asymmetric Fe– $\text{H}_2$  and Fe– $\text{D}_2$  stretching ( $\nu^{\uparrow\downarrow}$ ) bands are seen at much higher energies:  $1774$  and  $1276\text{ cm}^{-1}$  in  $1_{\text{H}}^{\text{H}_2}$  and  $1_{\text{D}}^{\text{D}_2}$ , respectively. The Fe–H stretching ( $\nu_{\uparrow}$ ) band for  $1_{\text{H}}^{\text{H}_2}$  is clearly observed in the spectrum at  $1915\text{ cm}^{-1}$ . The modes from  $1350$  to  $1410\text{ cm}^{-1}$  in 1-D are the  $\nu_{\uparrow}$  modes of the possible deuterium isotopologues and their decay products  $1_{\text{D}}^{\text{D}_2}$ ,  $1_{\text{D}}^*$ , and  $1_{\text{D}}^{\text{N}_2}$ . There is a weaker feature at  $\sim 1956\text{ cm}^{-1}$  for the 1-H sample, consistent with  $1_{\text{H}}^*$ . An admixture of  $1_{\text{H}}^{\text{N}_2}$  possibly results in a shoulder at  $\sim 1890\text{ cm}^{-1}$ , yet our calculations indicate that both  $\nu_{\uparrow}(1_{\text{H}}^{\text{H}_2})$  and  $\nu_{\uparrow}(1_{\text{H}}^{\text{N}_2})$  modes contribute to the same  $1915\text{ cm}^{-1}$  band. Here we note that the  $\nu_{\uparrow}(1_{\text{H}}^*)$  band at  $1956\text{ cm}^{-1}$  represents the highest observed NRVS frequency to date, and this augurs well for future studies aimed at the characterization of iron–hydride interactions. Further, it is important to note that the NRVS specificity for iron motion, high energy, and isolation of Fe– $\text{H}_x$  modes affords a strong handle on the quantitative composition of our NRVS spectrum with respect to adventitious subspecies  $1_{\text{H}}^*$  and  $1_{\text{H}}^{\text{N}_2}$ , which were anticipated by the IR data and supported by its DFT simulation (Figures S4 and S5). Finally, we note that, compared to the IR spectrum, identification of the hydrogen-based modes at these energies in NRVS (Figure 2a) is unambiguous.

In Figure 3, we present NRVS spectra for 1-H and 1-D in the range below  $1000\text{ cm}^{-1}$ , again compared with each other and with DFT simulations. As mentioned above, the Fe– $\text{H}_2$  bending modes are split by coupling with Fe–H motions in  $1_{\text{H}}^{\text{H}_2}$ . Thus, different frequencies and intensities are observed for in-plane ( $\delta$ ) and out-of-plane ( $\delta'$ ) Fe– $\text{H}_2$  bending depending on whether the associated Fe–H bending is in-phase ( $\leftarrow^{\ominus}$ ) or out-of-phase ( $\rightarrow^{\ominus}$ ), as depicted in Chart 1. Starting from high energy, an isotope-sensitive feature observed at  $823\text{ cm}^{-1}$  in 1-H is a coupled in-plane in-phase Fe– $\text{H}_2$  and Fe–H bending ( $\delta_{\leftarrow^{\ominus}}$ ) mode of  $1_{\text{H}}^{\text{H}_2}$  shown in Figure 3, top. The experimental feature at  $733\text{ cm}^{-1}$  in 1-H is consistent with Fe– $\text{H}_2$  and Fe–H out-of-plane in-phase bending ( $\delta'_{\leftarrow^{\ominus}}$ ) motion. In our calculations, this feature is derived from four modes with similar characters predicted in the  $726\text{--}732\text{ cm}^{-1}$  range, but with varying degrees of coupling to the dppe ligands. Because of this coupling with the outer coordination shell, these modes are sensitive to packing of the solid-state environment, which may account for the slight shoulder at  $728\text{ cm}^{-1}$  in the experimental spectrum of 1-H. The next two isotopically sensitive features at  $558$  and  $584\text{ cm}^{-1}$  in 1-H are identified as H–Fe– $\text{H}_2$  out-of-phase bending modes, out-of-plane ( $\delta'_{\rightarrow^{\ominus}}$ ) and in-plane ( $\delta_{\rightarrow^{\ominus}}$ ), respectively (Chart 1).

**Chart 1. Normal Modes Expected for a Trans Coordination of Dihydrogen and Hydride Ligands in an Idealized Iron(II) Octahedral Complex<sup>a</sup>**

307 ( $\text{cm}^{-1}$ )	573	616	845	860	1096	1726	1913	3129
$A_2 (C_{2v})$	$B_2$	$B_1$	$B_1$	$B_2$	$A_1$	$B_2$	$A_1$	$A_1$
$\tau^{\ominus}$	$\delta_{\rightarrow^{\ominus}}$	$\delta'_{\rightarrow^{\ominus}}$	$\delta'_{\leftarrow^{\ominus}}$	$\delta_{\leftarrow^{\ominus}}$	$\nu^{\uparrow\uparrow}$	$\nu^{\uparrow\downarrow}$	$\nu_{\uparrow}$	$\nu^{\uparrow\uparrow}$

<sup>a</sup>The nine modes are based on  $C_{2v}$ -symmetric  $\text{trans}[\text{Fe}(\eta^2\text{-H}_2)(\text{H})(\text{PH}_3)_4]^+$  ( $1_{\text{H}}^{\text{H}_2-C_{2v}}$ ) model calculations, as described in the Supporting Information and shown in Figure S1. Rows top to bottom: arrow-style mode representations; calculated frequencies ( $\text{cm}^{-1}$ );  $C_{2v}$  character names; arrow-based character names presently employed for  $1_{\text{H}}^{\text{H}_2}$  and its derivatives.

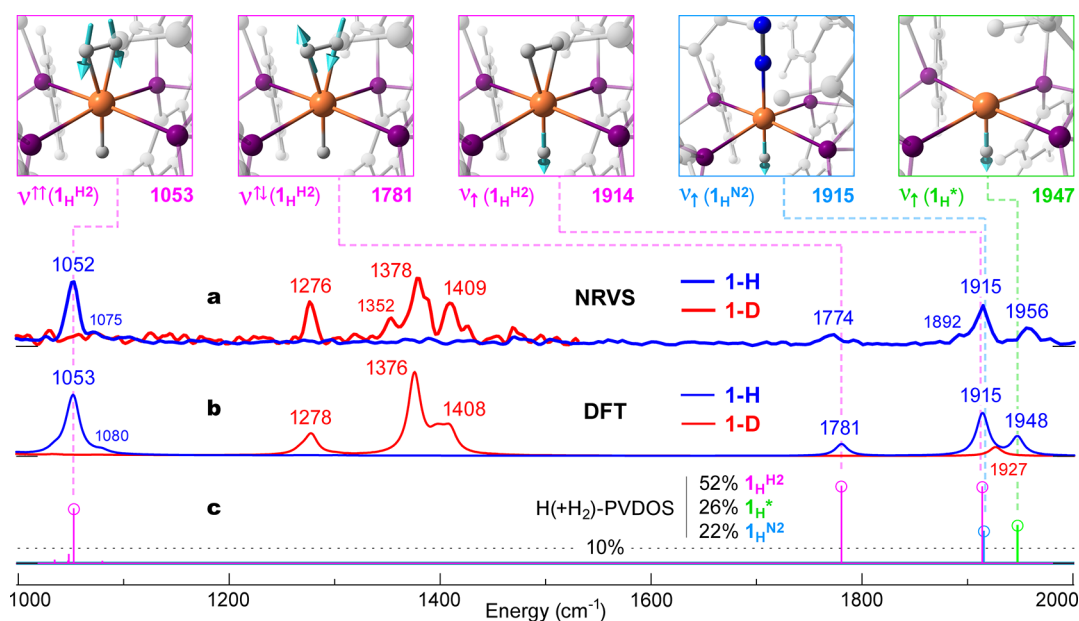


**Figure 2.** (a) Experimental NRVS data for high-energy (1000–2000  $\text{cm}^{-1}$ ) bands of samples 1-H and 1-D. (b) Collective DFT  $^{57}\text{Fe}$ -PVDOS simulations for 1-H including 52%  $1\text{-H}^{1\text{H}^2}$ , 26%  $1\text{-H}^*$ , and 22%  $1\text{-H}^{\text{N}2}$  and for 1-D using equivalent contributions from  $1\text{-D}^{\text{D}2}$ ,  $1\text{-D}^*$ , and  $1\text{-D}^{\text{N}2}$ . (c) DFT stick  $\text{H}(+\text{H}_2)$ -PVDOS intensities for the iron ligand hydride (and dihydrogen in  $1\text{-H}^{\text{H}2}$ ) nuclei in the three color-coded species of the 1-H sample, weighted with their composition factors. The composition (%) of the mixed sample was obtained based on the relative intensities of the experimental spectra bands in the 1000–2000  $\text{cm}^{-1}$  region, with individual contributions from the three pure calculated species shown in Figures S3 and S6–S7. Top: Predicted atomic motions from DFT simulations for normal modes with  $\text{H}(+\text{H}_2)$ -PVDOS > 10%. The mode-to-band associations are highlighted by broken lines.

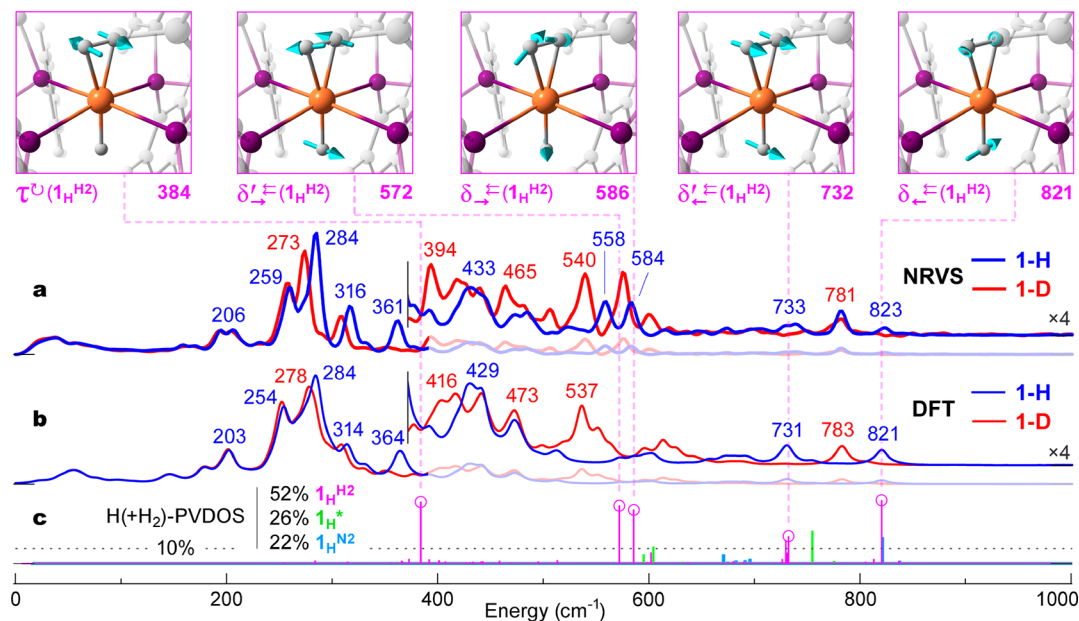


**Figure 3.** (a) Experimental NRVS data for low-energy (0–1000  $\text{cm}^{-1}$ ) bands of samples 1-H and 1-D. (b) DFT  $^{57}\text{Fe}$ -PVDOS simulations for 1-H and 1-D. (c) DFT stick  $\text{H}(+\text{H}_2)$ -PVDOS intensities in the three color-coded species of the 1-H sample, weighted with their composition factors. The 4 $\times$  intensity insets in parts a and b display spectra >370  $\text{cm}^{-1}$ . Top: Predicted atomic motions for selected normal modes of  $1\text{-H}^{1\text{H}^2}$  with  $\text{H}(+\text{H}_2)$ -PVDOS > 10%. Mode-to-band associations are highlighted by broken lines. Further figure details follow the legend of Figure 2.

The most prominent NRVS feature is located at 284/273  $\text{cm}^{-1}$  for 1-H/1-D (Figure 3a), with its intensity approximately 100 times higher (Figure S6a) than that of the high-energy Fe–H stretching band at 1915  $\text{cm}^{-1}$ . This global maximum in the spectra results from vibrations reminiscent of the intense transaxial bending modes of six-coordinate iron complexes with a 4-fold axis of symmetry.<sup>29,30</sup> In all of the calculated species, the DFT modes that produce the most intense  $\sim 250$ – $300$   $\text{cm}^{-1}$

region reveal entire  $[\text{H}/\text{D}-\text{Fe}(\text{H}_2/\text{D}_2)/(\text{N}_2)]$  axial fragment displacements approximately either parallel to the equatorial plane formed by the Fe–P bonds or perpendicular to this plane, as illustrated by animations in the Supporting Information.

Our analysis indicates that modes with significant contributions (>10%) from the H<sup>−</sup> and H<sub>2</sub> ligand motions do not supply 1-H spectral intensities at energies below  $\sim 570$   $\text{cm}^{-1}$  (Figure S6a), while the corresponding low-energy limit for the D<sup>−</sup> and

D<sub>2</sub> ligands in <sup>57</sup>Fe-PVDOS of **1-D** is ~260 cm<sup>-1</sup> (Figure S7a). For example, the strongest mode of rotational  $\tau^{\text{O}}(\mathbf{1}_H^{\text{H}_2})$  character is predicted at 384 cm<sup>-1</sup> but conveys only negligible Fe motion (Figures 3 and S6b). However, at 392 cm<sup>-1</sup>, there is a satellite mode calculated with similar, but much weaker, H<sub>2</sub> rotational character that contains <sup>57</sup>Fe-PVDOS and agrees well with the shoulder at the same position in the experimental spectrum of **1-H**. Inspection of the 392 cm<sup>-1</sup> normal-mode displacements indicates it acquires intensity through coupling with equatorial Fe–P motion. The nearby isotopically sensitive intensities in **1-H** at 316, 332 (shoulder), and 361 cm<sup>-1</sup> are calculated at 314, 333, and 364 cm<sup>-1</sup> containing varying Fe–P stretching motions, and similarly to the 284 cm<sup>-1</sup> mode, near-concerted translation of the H–Fe–H<sub>2</sub> moiety within the Fe–P plane. The second greatest intensity in the spectrum is at 259 cm<sup>-1</sup> in **1-H**, and it is primarily correlated with P–Fe–P out-of-plane bending motion where H–Fe–H<sub>2</sub> is collectively translating through the equatorial plane.

In summary, we have characterized *trans*-[<sup>57</sup>Fe( $\eta^2$ -H<sub>2</sub>)(H)-(dppe)<sub>2</sub>][BPh<sub>4</sub>] using <sup>57</sup>Fe-NRVS combined with DFT calculations. The Fe–H stretching modes in this compound and its H<sub>2</sub>-loss byproduct represent the highest energy vibrational features ever observed by NRVS. Moreover, our combined approach developed a complete picture of the H–Fe–H<sub>2</sub> vibrational structure even in the congested low-energy regime. This implies that hydrogen motion in this low-energy region can serve as a surrogate probe in systems that are not yet capable of being explored with high-energy NRVS. There are clear accessible applications to the study of hydrogen storage materials, for example, iron-containing metal–organic frameworks, where the presence of framework hydrogen limits neutron-based approaches.<sup>31</sup> Extension of this work to dilute biological systems is challenging, but with continued improvements in synchrotron radiation X-ray production, it will eventually be possible to characterize Fe–H<sub>2</sub> vibrational modes in enzyme intermediates.

## ■ ASSOCIATED CONTENT

### SI Supporting Information

The Supporting Information is available free of charge at <https://pubs.acs.org/doi/10.1021/acs.inorgchem.0c03006>.

Experimental and computational procedures and supplementary figures and tables (PDF)

Animations showing the calculated normal modes with significant <sup>57</sup>Fe proton PVDOS character (ZIP)

Animations showing the calculated normal modes with significant iron-bound proton PVDOS character (ZIP)

Cartesian coordinates of the optimized structures (ZIP)

## ■ AUTHOR INFORMATION

### Corresponding Authors

Ming-Hsi Chiang – *Institute of Chemistry, Academia Sinica, Nankang, Taipei 115, Taiwan*; [orcid.org/0000-0002-7632-9369](https://orcid.org/0000-0002-7632-9369); Email: [chiangmh@gate.sinica.edu.tw](mailto:chiangmh@gate.sinica.edu.tw)

Vladimir Pelmentschikov – *Institut für Chemie, Technische Universität Berlin, Berlin 10623, Germany*; [orcid.org/0000-0002-0523-4418](https://orcid.org/0000-0002-0523-4418); Email: [pelmentschikov@tu-berlin.de](mailto:pelmentschikov@tu-berlin.de)

Stephen P. Cramer – *SETI Institute, Mountain View, California 94043, United States*; [orcid.org/0000-0002-3751-7623](https://orcid.org/0000-0002-3751-7623); Email: [scramer@seti.org](mailto:scramer@seti.org)

## Authors

Leland B. Gee – *Department of Chemistry, Stanford University, Stanford, California 94305, United States*; [orcid.org/0000-0002-5817-3997](https://orcid.org/0000-0002-5817-3997)

Yu-Chiao Liu – *Institute of Chemistry, Academia Sinica, Nankang, Taipei 115, Taiwan*; [orcid.org/0000-0001-6055-8039](https://orcid.org/0000-0001-6055-8039)

Chang-Chih Hsieh – *Institute of Chemistry, Academia Sinica, Nankang, Taipei 115, Taiwan*

Hongxin Wang – *SETI Institute, Mountain View, California 94043, United States*

Yoshitaka Yoda – *Precision Spectroscopy Division, SPring-8/JASRI, Sayo, Hyogo 679-5198, Japan*

Hiroaki Matsuura – *Life Science Research Infrastructure Group, Advanced Photon Technology Division, RIKEN/SPring-8 Center, Sayo-gun, Hyogo 679-5148, Japan*

Lei Li – *Hyogo Science and Technology Association, Synchrotron Radiation Research Center, Tatsuno-shi, Hyogo 679-5165, Japan*

Complete contact information is available at: <https://pubs.acs.org/doi/10.1021/acs.inorgchem.0c03006>

## Author Contributions

<sup>†</sup>These authors contributed equally.

## Notes

The authors declare no competing financial interest.

## ■ ACKNOWLEDGMENTS

M.-H.C., Y.-C.L., and C.-C.H. acknowledge funding by the Ministry of Science and Technology of Taiwan and Academia Sinica (Grants AS-SS-108-02-1, AS-iMate-109-22, and AS-SS-109-07). V.P. was funded by the Deutsche Forschungsgemeinschaft (German Research Foundation) under Germany's Excellence Strategy EXC 2008-390540038 UniSysCat. S.P.C. was funded by National Institutes of Health Grant GM65440. NRVS data was measured at SPring-8 under proposals 2018B1379 and 2019A1259 (JASRI). Some computational work was performed under the XSIM project on the CORI computing system at NERSC, a U.S. Department of Energy Office of Science User Facility operated under Contract DE-AC02-05CH11231.

## ■ REFERENCES

- (1) Kubas, G. J.; Ryan, R. R.; Swanson, B. I.; Vergamini, P. J.; Wasserman, H. J. Characterization of the 1st Examples of Isolable Molecular-Hydrogen Complexes, Mo(CO)<sub>3</sub>(Pcy<sub>3</sub>)<sub>2</sub>(H<sub>2</sub>), W(CO)<sub>3</sub>(Pcy<sub>3</sub>)<sub>2</sub>(H<sub>2</sub>), Mo(CO)<sub>3</sub>(Pi-Pr<sub>3</sub>)<sub>2</sub>(H<sub>2</sub>), W(CO)<sub>3</sub>(Pi-Pr<sub>3</sub>)<sub>2</sub>(H<sub>2</sub>) - Evidence for a Side-On Bonded H<sub>2</sub> Ligand. *J. Am. Chem. Soc.* **1984**, *106* (2), 451–452.
- (2) Kubas, G. J. Activation of dihydrogen and coordination of molecular H<sub>2</sub> on transition metals. *J. Organomet. Chem.* **2014**, *751*, 33–49.
- (3) Bullock, R. M.; Appel, A. M.; Helm, M. L. Production of hydrogen by electrocatalysis: making the H-H bond by combining protons and hydrides. *Chem. Commun.* **2014**, *50* (24), 3125–3143.
- (4) Kubas, G. J. Hydrogen activation on organometallic complexes and H<sub>2</sub> production, utilization, and storage for future energy. *J. Organomet. Chem.* **2009**, *694* (17), 2648–2653.
- (5) Haumann, M.; Stripp, S. T. The Molecular Proceedings of Biological Hydrogen Turnover. *Acc. Chem. Res.* **2018**, *51* (8), 1755–1763.
- (6) Lubitz, W.; Ogata, H.; Rudiger, O.; Reijerse, E. Hydrogenases. *Chem. Rev.* **2014**, *114* (8), 4081–4148.

- (7) Peters, J. W.; Schut, G. J.; Boyd, E. S.; Mulder, D. W.; Shepard, E. M.; Broderick, J. B.; King, P. W.; Adams, M. W. W. [FeFe]- and [NiFe]-hydrogenase diversity, mechanism, and maturation. *Biochim. Biophys. Acta, Mol. Cell Res.* **2015**, *1853* (6), 1350–1369.
- (8) Crabtree, R. H. Dihydrogen Complexation. *Chem. Rev.* **2016**, *116* (15), 8750–8769.
- (9) Kaesz, H. D.; Saillant, R. B. Hydride Complexes of Transition Metals. *Chem. Rev.* **1972**, *72* (3), 231–281.
- (10) Heinekey, D. M.; Oldham, W. J. Coordination Chemistry of Dihydrogen. *Chem. Rev.* **1993**, *93* (3), 913–926.
- (11) Woinska, M.; Grabowsky, S.; Dominiak, P. M.; Wozniak, K.; Jayatilaka, D. Hydrogen atoms can be located accurately and precisely by x-ray crystallography. *Sci. Adv.* **2016**, *2* (5), e1600192.
- (12) Perutz, R. N.; Procacci, B. Photochemistry of Transition Metal Hydrides. *Chem. Rev.* **2016**, *116* (15), 8506–8544.
- (13) Seto, M.; Yoda, Y.; Kikuta, S.; Zhang, X. W.; Ando, M. Observation of Nuclear Resonant Scattering Accompanied by Phonon Excitation Using Synchrotron Radiation. *Phys. Rev. Lett.* **1995**, *74*, 3828–3831.
- (14) Chumakov, A.; Rüffer, R. Nuclear inelastic scattering. *Hyperfine Interact.* **1998**, *113* (1), 59–79.
- (15) Scheidt, W. R.; Li, J. F.; Sage, J. T. What Can Be Learned from Nuclear Resonance Vibrational Spectroscopy: Vibrational Dynamics and Hemes. *Chem. Rev.* **2017**, *117* (19), 12532–12563.
- (16) Cramer, S. P. Nuclear Resonance Vibrational Spectroscopy. *X-Ray Spectroscopy with Synchrotron Radiation: Fundamentals and Applications*; Springer International Publishing: Cham, Switzerland, 2020; Chapter 10, pp 257–278.
- (17) Sage, J. T.; Paxson, C.; Wyllie, G. R. A.; Sturhahn, W.; Durbin, S. M.; Champion, P. M.; Alp, E. E.; Scheidt, W. R. Nuclear resonance vibrational spectroscopy of a protein active-site mimic. *J. Phys.: Condens. Matter* **2001**, *13*, 7707–7722.
- (18) Leu, B. M.; Zgierski, M. Z.; Wyllie, G. R. A.; Scheidt, W. R.; Sturhahn, W.; Alp, E. E.; Durbin, S. M.; Sage, J. T. Quantitative Vibrational Dynamics of Iron in Nitrosyl Porphyrins. *J. Am. Chem. Soc.* **2004**, *126* (13), 4211–4227.
- (19) Gee, L. B.; Pelmenschikov, V.; Wang, H.; Mishra, N.; Liu, Y.-C.; Yoda, Y.; Tamasaku, K.; Chiang, M.-H.; Cramer, S. P. Vibrational and electronic characterization of a diiron bridging hydride complex – a model for hydrogen catalysis. *Chem. Sci.* **2020**, *11* (21), 5487–5493.
- (20) Ogata, H.; Krämer, T.; Wang, H.; Schilter, D.; Pelmenschikov, V.; van Gastel, M.; Neese, F.; Rauchfuss, T. B.; Gee, L. B.; Scott, A. D.; Yoda, Y.; Tanaka, Y.; Lubitz, W.; Cramer, S. P. Hydride bridge in [NiFe]-hydrogenase observed by nuclear resonance vibrational spectroscopy. *Nat. Commun.* **2015**, *6* (1–8), 7890.
- (21) Reijerse, E. J.; Pham, C. C.; Pelmenschikov, V.; Gilbert-Wilson, R.; Adamska-Venkatesh, A.; Siebel, J. F.; Gee, L. B.; Yoda, Y.; Tamasaku, K.; Lubitz, W.; Rauchfuss, T. B.; Cramer, S. P. Direct observation of an iron bound terminal hydride intermediate in [FeFe] hydrogenase. *J. Am. Chem. Soc.* **2017**, *139* (12), 4306–4309.
- (22) Pelmenschikov, V.; Birrell, J. A.; Pham, C. C.; Mishra, N.; Wang, H. X.; Sommer, C.; Reijerse, E.; Richers, C. P.; Tamasaku, K.; Yoda, Y.; Rauchfuss, T. B.; Lubitz, W.; Cramer, S. P. Reaction Coordinate Leading to H<sub>2</sub> Production in [FeFe] Hydrogenase Identified by Nuclear Resonance Vibrational Spectroscopy and Density Functional Theory. *J. Am. Chem. Soc.* **2017**, *139* (46), 16894–16902.
- (23) Pham, C. C.; Mulder, D. W.; Pelmenschikov, V.; King, P. W.; Ratzloff, M. W.; Wang, H.; Mishra, N.; Alp, E. E.; Zhao, J.; Hu, M. Y.; Tamasaku, K.; Yoda, Y.; Cramer, S. P. Terminal Hydride Species in [FeFe]-Hydrogenases are Vibrationally Coupled to the Active Site Environment. *Angew. Chem., Int. Ed.* **2018**, *57*, 10605–10609.
- (24) Pelmenschikov, V.; Gee, L. B.; Wang, H.; MacLeod, K. C.; McWilliams, S. F.; Skubi, K. L.; Cramer, S. P.; Holland, P. L. High-Frequency Fe–H Vibrations in a Bridging Hydride Complex Characterized by NRVS and DFT. *Angew. Chem., Int. Ed.* **2018**, *57* (30), 9367–9371.
- (25) Abrecht, D. G.; Munoz, J. A.; Smith, H. L.; Fultz, B. Spin-State Effects on the Thermal Dihydrogen Release from Solid-State [MH( $\eta^2$ -H<sub>2</sub>)dppe<sub>2</sub>]<sup>+</sup> (M = Fe, Ru, Os) Organometallic Complexes for Hydrogen Storage Applications. *J. Phys. Chem. C* **2014**, *118* (4), 1783–1792.
- (26) Ricci, J. S.; Koetzle, T. F.; Bautista, M. T.; Hofstede, T. M.; Morris, R. H.; Sawyer, J. F. Single-Crystal X-Ray and Neutron Diffraction Studies of an  $\eta^2$ -Dihydrogen Transition-Metal Complex: *trans*-[Fe( $\eta^2$ -H<sub>2</sub>)(H)(PPH<sub>2</sub>CH<sub>2</sub>CH<sub>2</sub>PPH<sub>2</sub>)<sub>2</sub>]BPh<sub>4</sub>. *J. Am. Chem. Soc.* **1989**, *111* (24), 8823–8827.
- (27) Bautista, M. T.; Cappellani, E. P.; Drouin, S. D.; Morris, R. H.; Schweitzer, C. T.; Sella, A.; Zubkowski, J. Preparation and Spectroscopic Properties of the Eta-2-Dihydrogen Complexes [Mh-(Eta-2-H<sub>2</sub>)(Pr<sub>2</sub>ch<sub>2</sub>ch<sub>2</sub>pr<sub>2</sub>)<sub>2</sub>]<sup>+</sup> (M = Fe, Ru, R = Ph, Et) and Trends in Properties down the Iron Group Triad. *J. Am. Chem. Soc.* **1991**, *113* (13), 4876–4887.
- (28) Kubas, G. J. Fundamentals of H<sub>2</sub> binding and reactivity on transition metals underlying hydrogenase function and H<sub>2</sub> production and storage. *Chem. Rev.* **2007**, *107* (10), 4152–4205.
- (29) Bell, C. B.; Wong, S. D.; Xiao, Y.; Klinker, E. J.; Tenderholt, A. L.; Smith, M. C.; Rohde, J.-U.; Que, L.; Cramer, S. P.; Solomon, E. I. A combined NRVS and DFT study of Fe(IV)=O model complexes: a diagnostic method for the elucidation of non-heme iron enzyme intermediates. *Angew. Chem., Int. Ed.* **2008**, *47* (47), 9071–9074.
- (30) Zeng, W.; Barabanschikov, A.; Zhang, Y.; Zhao, J.; Sturhahn, W.; Alp, E. E.; Sage, J. T. Synchrotron-Derived Vibrational Data Confirm Unprotonated Oxo Ligand in Myoglobin Compound II. *J. Am. Chem. Soc.* **2008**, *130* (6), 1816–1817.
- (31) Gygi, D.; Bloch, E. D.; Mason, J. A.; Hudson, M. R.; Gonzalez, M. I.; Siegelman, R. L.; Darwish, T. A.; Queen, W. L.; Brown, C. M.; Long, J. R. Hydrogen Storage in the Expanded Pore Metal–Organic Frameworks M<sub>2</sub>(dobpdc) (M = Mg, Mn, Fe, Co, Ni, Zn). *Chem. Mater.* **2016**, *28* (4), 1128–1138.